Arabian Journal of Chemistry (2023) **16**, 104613

King Saud University

Arabian Journal of Chemistry

www.ksu.edu.sa
www.sciencedirect.com

ORIGINAL ARTICLE

Fabrication of a novel electrochemical sensor based on tin disulfide/multi-walled carbon nanotunbes-modified electrode for rutin determination in natural vegetation

Ying Liang [a,c], Lingyu Zhang [c], Hongmei Wang [b,d], Xinru Cai [c], Li Zhang [c], Yixin Xu [c], Chunxia Yao [b,*], Wenshuai Si [b,*], Zhipeng Huang [a,*], Guoyue Shi [e]

[a] *School of Chemical Science and Engineering, Tongji University, Shanghai 200092, PR China*
[b] *Institute for Agro-food Standards and Testing Technology, Shanghai Key Laboratory of Protected Horticultural Technology, Laboratory of Quality and Safety Risk Assessment for Agro-products (Shanghai), Ministry of Agriculture, Shanghai Academy of Agricultural Sciences, 1000 Jingqi Road, Shanghai 201403, China*
[c] *School of Pharmacy, Shanghai University of Medicine and Health Sciences, Shanghai 201318, PR China*
[d] *College of Marine Ecology and Environment, Shanghai Ocean University, Shanghai 201306, China*
[e] *Department of Chemistry, East China Normal University, 500 Dongchuan Road, Shanghai 200241, China*

Received 11 April 2022; accepted 18 January 2023
Available online 26 January 2023

KEYWORDS

Tin disulfide;
Multi-walled carbon nanotubes;
Electrochemical sensor;
Rutin

Abstract A tin disulfide and multi-walled carbon nanotube (SnS_2/CNTs) electrochemical sensor was constructed for the sensitive and selective determination of rutin in plants. Tin disulfide nanoflowers with various particle sizes were prepared by controlling the reaction time and composited with multi-walled CNTs. The morphology, crystal structure, and chemical composition of these SnS_2/CNTs composites were characterized using XRD, XPS, and SEM-EDS. Results illustrated that the SnS_2/CNTs had a large specific surface area, good conductivity, and remarkable electrocatalytic performance. The pH of the buffer solution, the scanning rate, and the amount of modified material were also optimized for the rapid detection of rutin. A 2-electron-2-proton mechanism, involving a few rapid and consecutive stages, was speculated to occur during rutin oxidation, based on the observed slope of -53 mV/pH. There was an appreciable linear relationship between the reductive peak current from DPV and the rutin concentration, ranging from 0.005-0.05 μmol/L and 0.1-6 μmol/L, with a detection limit of 0.22 nmol/L (S/N = 3). The sensor also demonstrated

* Corresponding authors.
E-mail addresses: 67749801@qq.com (C. Yao), siwenshuai021@163.com (W. Si), zphuang@tongji.edu.cn (Z. Huang).
Peer review under responsibility of King Saud University.

Production and hosting by Elsevier

https://doi.org/10.1016/j.arabjc.2023.104613

good selectivity, excellent sensitivity, and reproducibility when analyzing rutin in real plant samples, with satisfactory recovery, and was also highly consistent with results of HPLC, and thus could be used to evaluate the medicinal value of natural vegetation.

1. Introduction

Rutin (vitamin P) is widely found in natural vegetation such as buckwheat, red date, and wolfberry (Al-Harbi et al., 2019; Liu et al., 2017a), and possesses several medical applications such as treating bleeding, digestive system problems, and high blood pressure (Shi et al., 2022; Sghaier et al., 2016). Therefore, quantifying the content of rutin in natural vegetation is essential to assessing and developing their medicinal value. Various analytical methods have been proposed for the qualitative and quantitative analysis of rutin, such as high-performance liquid chromatography (Kalinová et al., 2018), colorimetry (Jjgyasa, 2018), fluorescence spectrometry (Sasikumar et al., 2021), and capillary electrophoresis (Wang et al., 2016). Among these, the electrochemical method has the advantages of a fast response, low cost, simple equipment, and high sensitivity, making it suitable for the rapid detection of trace rutin in natural vegetation and evaluating the medicinal value of plants (Liang et al., 2022; Xie et al., 2022; Incebay et al., 2022; Saylakcı et al., 2021; İncebay et al., 2017; Kilic et al., 2020).

Suitable electrode materials are key to the efficient detection of rutin using electrochemical sensors, and transition metal sulfides have attracted significant attention due to their excellent physical and chemical properties (Liang et al., 2019; Diao et al., 2020; Kubendhiran et al., 2018a; Sakthivel et al., 2019). In particular, tin disulfide (SnS_2) has a unique layered structure as well as favorable optical, electrical, and electrochemical properties. It has thus been widely used in sensors and lithium-ion batteries (Xu et al., 2014; Sakthivel et al., 2019; Wang et al., 2013). SnS_2 materials possess various morphologies, such as nanoparticles (Jiang et al., 2016), nanosheets (Mondal et al., 2021), nanoribbons (Liu et al., 2017b), and nanoflowers (Yin et al., 2019). Of these, it has been reported that application of the hierarchical nanoflower structure of SnS_2 as an electrode material can effectively improve electrochemical performance. The large specific surface area of SnS_2 promotes a fast rate of electron transfer, making it an excellent choice for the preparation of modified electrodes.

However, because SnS_2 nanoparticles are prone to aggregation, which results in a reduced the electron transfer rate and affects the electrochemical performance, their use in electrode modification materials can be limited (Sakthivel et al., 2019). To overcome such issues, a combination of carbon nanotubes and other nanomaterials are often added when fabricating electrochemical sensors. The presence of carbon nanomaterials can not only retard aggregation and improve the structural stability of SnS_2 nanoflowers, but also improve the conductivity and sensitivity of the sensor (Pham et al., 2017; Clancy et al., 2018; Xue et al., 2016; Wang et al., 2021). As a result, integrating multi-walled carbon nanotubes and SnS_2 to create synergistic effects can improve selectivity and activity in electrochemical sensors.

Based on previous reports and to the best of our knowledge, there have been no reports on the use of tin disulfide nanomaterials and multi-walled carbon nanotubes with high selectivity and sensitivity for rutin detection in natural vegetation to evaluate the medicinal value of plants. In this work, three types of SnS_2 nanomaterials with different particle sizes were prepared, and their structure, crystal phase, and morphology were characterized by X-ray diffraction (XRD), X-ray photoelectron spectroscopy (XPS), and scanning electron microscopy (SEM). In addition, cyclic voltammetry (CV) and differential pulse voltammetry (DPV) were utilized to optimize other aspects of electrochemical detection, including the pH of the buffer solution, the scanning rate, and the amount of modified material by an SnS_2/CNTs electrochemical sensor, to realize the enhanced sensitivity and efficient electrochemical detection of rutin in the presence of common interferents. Subsequently, the viability of rutin detection was demonstrated using plant samples, which proved the feasibility of the SnS_2/CNTs electrochemical sensor.

2. Experimental section

2.1. Materials and reagents

Multi-walled CNTs were purchased from Adamas Co. ltd. Rutin, thioacetamide, anhydrous stannic chloride, ethanol, potassium ferricyanide, potassium hexacyanoferrate (II), sodium dihydrogen phosphate, dibasic sodium phosphate, potassium chloride, nitric acid, sodium hydroxide, and acetone were purchased from Sigma-Aldrich Chemical Co., China. All chemicals were analytically pure and used without further purification. The phosphate buffer solution (PBS, 0.1 M) was composed of NaH_2PO_4 and Na_2HPO_4 mixed with distilled water.

2.2. Instruments and measurements

A CHI 660E electrochemical workstation was used to conduct the electrochemical experiment in a voltametric cell (10 mL) at room temperature. The three-electrode cell consisted of an SnS_2/CNT-modified glassy carbon electrode (GCE) as the working electrode, a platinum wire as the auxiliary electrode, and a saturated calomel electrode (SCE) as the reference electrode. The above instruments were purchased from Chenhua Instruments Co., China. XRD was measured using a max-2600PC via ceramic-monochromatic Cu K, operating at 45 kV and 20 mA, with a scanning rate of 5° per min in 2θ and a scanning range from 20 to 65°. XPS was performed for elemental analysis with a 60 W monochromatic Mg Kα source. The binding energy was calibrated based on the carbon 1 s peak at 284.6 eV. SEM images were obtained using a Hitachi Regulus 8100, and the energy dispersive spectrometer (EDS) spectra were recorded using an EDAX EDS Element. The TEM images, selective area electron diffraction (SAED) patterns, and low-magnification scanning TEM (STEM) images were obtained using a Titan Cubed Themis G2 300 (FEI) instrument.

2.3. Synthesis of tin disulfide/multi-walled carbon nanotube composites

Anhydrous tin tetrachloride (0.05 M) and thioacetamide (0.15 M) were dissolved in anhydrous ethanol (240 mL), and ultrasonically treated for 2 min to obtain a clear solution. The solution was heated for 4 h, 6 h, and 8 h at 60 °C to obtain 4h-SnS_2, 6h-SnS_2, and 8 h-SnS_2 samples, respectively, which were cooled down, centrifuged for 10 min, and then washed

with deionized water and ethanol. Finally, all samples were dried in a vacuum furnace at 60 °C to obtain dry brownish-yellow solids. SnS_2/CNT composites were prepared by dispersing carboxylated multi-walled carbon nanotubes and tin disulfide (ratio = 1:1) in ethanol.

2.4. Fabrication of 4h-SnS_2/CNTs-modified electrode

The 0.05 μm and 0.3 μm alumina slurries were placed on suede and dissolved with twice-distilled water to form a suspension, and then the glassy carbon electrode was carefully polished for 3 min. The electrode surface was cleaned after immersion in ethanol, acetone, and twice-distilled water for ultrasonic oscillation cleaning for 5 min. Finally, a bright mirror was obtained. Next, 5 μL of the 4 h-SnS_2/CNTs composite with ethanol was dropped onto the electrode surface and dried under an infrared lamp to obtain the 4h-SnS_2/CNTs modified electrode, which was gently rinsed with twice-distilled water.

2.5. Optimization of the experimental conditions

The experimental conditions of the SnS_2/CNT electrodes, including the pH of the buffer solution, the amount of modified material, and the scanning rate, were optimized to determine the rapid detection of rutin.

First, the 4h-SnS_2/CNTs/GCE surface was immersed in 0.05 mol/L PBS at different pH values (pH 2.3, 3, 4, 5, and 6), in which the concentration of rutin was 5.0 μmol/L. Then, the immersed electrode was applied by CV, which was performed in the range of 0.1 V to 0.8 V at a scan rate of 100 mV and sample interval of 0.001 V.

Second, the 4h-SnS_2/CNTs composite with different modification amounts (1 μL, 2 μL, 3 μL, 4 μL, 5 μL, and 6 μL) was dropped onto the electrode surface and dried under an infrared lamp, which was gently rinsed with twice-distilled water. The modified electrode was immersed in 5.0 μmol/L rutin solution, 0.05 mol/L PBS, and pH of 3.0. CV was recorded on the electrodes in the potential range between 0.1 and 0.8 V at a scan rate of 100 mV/s.

Thirdly, the CV of 5.0 μmol/L of rutin at different scanning rates (40 mV/s, 60 mV/s, 80 mV/s, 100 mV/s, 120 mV/s, 140 mV/s, and 160 mV/s) was recorded. Then, the reproducibility test was performed using three different GC electrodes under the exact same conditions. Repeatability and stability tests were also performed multiple times using the same electrode for rutin detection.

2.6. Preparation of plant samples before determination

The feasibility of the sensor was ascertained using 9 different natural plant samples including red date, black fruit wolfberry, asparagus, wolfberry, grape peel, tangerine, eggplant peel, buckwheat and apples. The plant samples were prepared for analysis according to reference (Liao et al., 2015). To prepare the samples for testing, the stems and soil of the fresh vegetables were removed for later use. All samples were crushed, freeze-dried, and passed through a 40–60 mesh sieve. Then, 0.5 g of sample (accurate to 0.0001 g) was added to 70 % ethanol (12.5 mL) and then sonicated for 15 min (150 W, 20 ℃, 60 ~ 62 KHz). After sonication, the samples were centrifuged for 5 min, and finally, the supernatant was filtered with a 0.45 μm filter membrane for later use.

3. Results and discussion

3.1. Characterization of the SnS_2/CNTs composites by XRD, XPS, SEM-EDS, and TEM

SnS_2 nanoparticles were prepared by the chemical bath deposition method, and their sizes were controlled by controlling reaction times. The crystal phases of the SnS_2/CNTs composites and SnS_2 nanoparticles were characterized by XRD (Fig. 1). In comparison to the standard card (JCPDS 23–667), the peak height, peak shape, and peak angle of 4h-SnS_2, 6h-SnS_2, 8 h-SnS_2 nanoparticles were the same, and their characteristic diffraction peaks coincided. It was also found that in these materials, longer reaction times resulted in smaller half peak widths and larger grain sizes. Interestingly, compared to the XRD patterns observed in the CNTs, the diffraction peaks located at the 2θ angle of 25.8° were regenerated in the SnS_2/CNTs, which represented the (0 0 2) diffraction planes (Sakthivel et al., 2019) according to the periodicity between the graphene layers (Reznik et al., 1995). These peaks confirmed successful composite formation. In addition, in order to study the interaction between SnS_2 nanoparticles and CNTs, zeta potential was measured. Zeta potential is related to the surface charge and electric double layer of nanoparticles, which can be used to explain functional group performance, adsorption/desorption phenomena, chemical surface modification or stability. The potentials of SnS_2 particles and CNTs are (1.29 ± 0.58) mv and (-2.86 ± 0.92) mV respectively. Therefore, they could combine through electrostatic attraction.

To evaluate the chemical composition, purity, integrity, and state of surface oxidation of the 4h-SnS_2/CNTs composites, XPS was applied to determine the binding energy of the elements in the micro and nano materials (Kubendhiran et al., 2018a). The XPS survey scan spectra and characteristic peaks for the Sn 3d, S 2p, and C 1 s levels in the 4h-SnS_2/CNT composites were as shown in Fig. 2. The peaks at 494.8 eV and

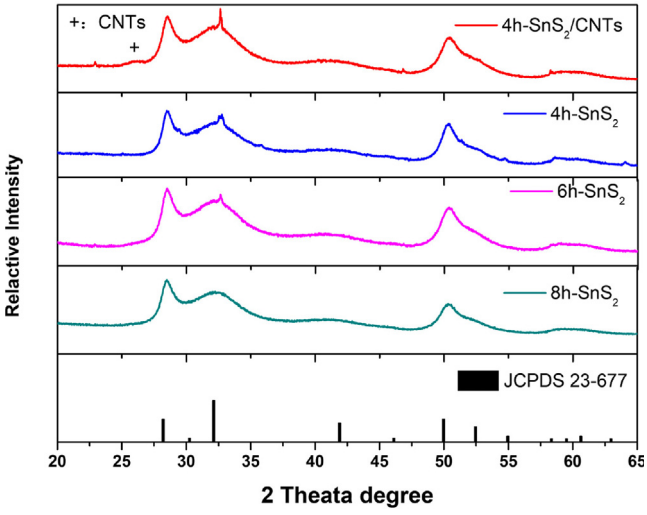

Fig. 1 XRD patterns of the SnS_2/CNTs and SnS_2 nanoflowers according to the standard card (JCPDS 23–667).

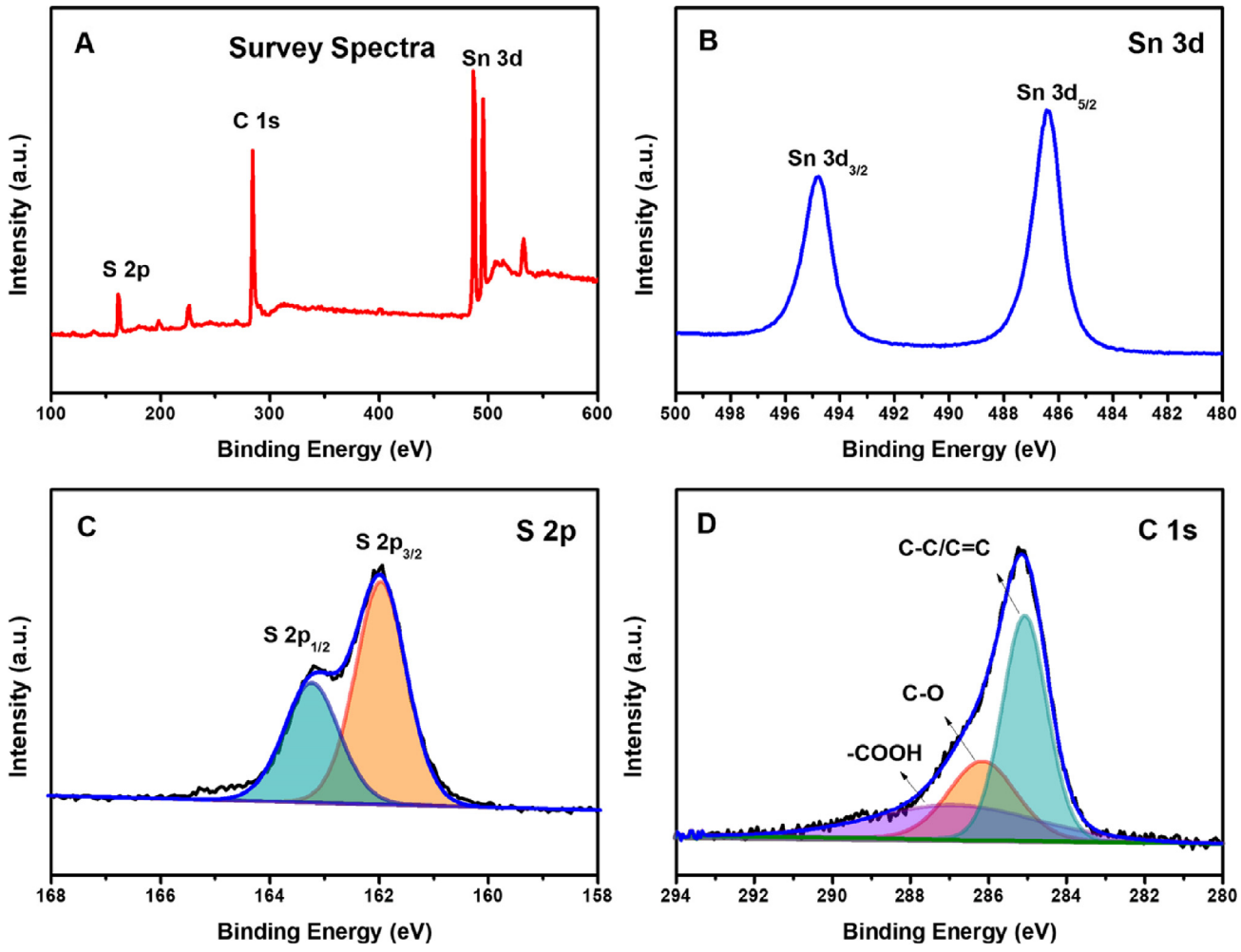

Fig. 2 (A) XPS survey spectrum of the 4h-SnS_2/CNTs; core level spectrum of (B) Sn 3d, (C) S 2p, (D) C 1 s.

486.4 eV (Fig. 2B) correspond to the Sn $3d_{3/2}$ and $Sn3d_{5/2}$ spin–orbit spin components of Sn^{4+} in SnS_2 (Wang et al., 2017; Xu et al., 2019). In addition, the high-resolution scan of S 2p unambiguously represents two major peaks due to S $2p_{1/2}$ at 163.2 eV and S $2p_{3/2}$ at 162.0 eV, separately shown in Fig. 2C (Huang et al., 2018). As shown in Fig. 2D, the three dominant peaks of the C 1 s at 285.0 eV, 286.1 eV, and 287.0 eV could be allocated to the non-oxygenated ring carbon (C—C/C=C,), the carbon in the C—O bonds, and the carbon in the —COOH bond, respectively (Kubendhiran et al., 2018b; Zhou et al., 2015).

The low-resolution SEM images (Fig. 3A–C) reveal that morphologically, the 4h-SnS_2, 6h-SnS_2, and 8 h-SnS_2 nanoparticles consisted of flower-like microspheres with a smooth surface. The size of these flower-like microspheres increased with the increase of the reaction time. The SEM images of 4h-SnS_2/CNTs (Fig. 3D) and 4h-SnS_2 (Fig. 3A) indicated that CNTs were uniformly adsorbed on the surface of these microspheres, thus resolving the aggregation problem of CNTs and increasing the specific surface area of the modified materials. In addition, the TEM images of the nanoparticles and the nanoparticle/CNTs materials obtained to verify the size distribution of the SnS_2, 4h-SnS_2, 6h-SnS_2, and 8 h-SnS_2 nanoparticles were as shown in Fig S1. The size of the flower-like microspheres increased with increasing reaction time. Moreover, as shown in Fig. S1D, it was observed that carbon nanotubes covered the nanoflower-like SnS_2 structures in the SnS_2/CNTs composites. The obtained TEM images corroborated the SEM images, both confirming the formation and presence of the SnS_2/CNTs composites. To further confirm that the synthesized materials were SnS_2 and 4h-SnS_2/CNTs, their elemental weight distributions and atomic contents were analyzed by SEM-EDS, and results were as shown in Fig. 3. The atomic ratio of tin and sulfur in these two materials was approximately 1:2, as given in Table S1, and a high proportion of carbon was found in the SnS_2/CNTs, indicating the successful synthesis of both SnS_2 and 4h-SnS_2/CNTs.

3.2. Electrochemical behavior

3.2.1. Electrochemical characterization of SnS_2 and SnS_2/CNTs-modified electrodes

To investigate the performances of the modified electrodes, bare GCE, 4h-SnS_2/GCE, 6h-SnS_2/GCE, 8 h-SnS_2/GCE, CNTs/GCE, and 4h-SnS_2/CNTs/GCE were scanned in a $K_3[Fe(CN)_6]/K_4[Fe(CN)_6]$ solution (5 mmol/L) using cyclic voltammetry (CV). The electrochemical performances of the modified electrodes were analyzed by comparing their redox

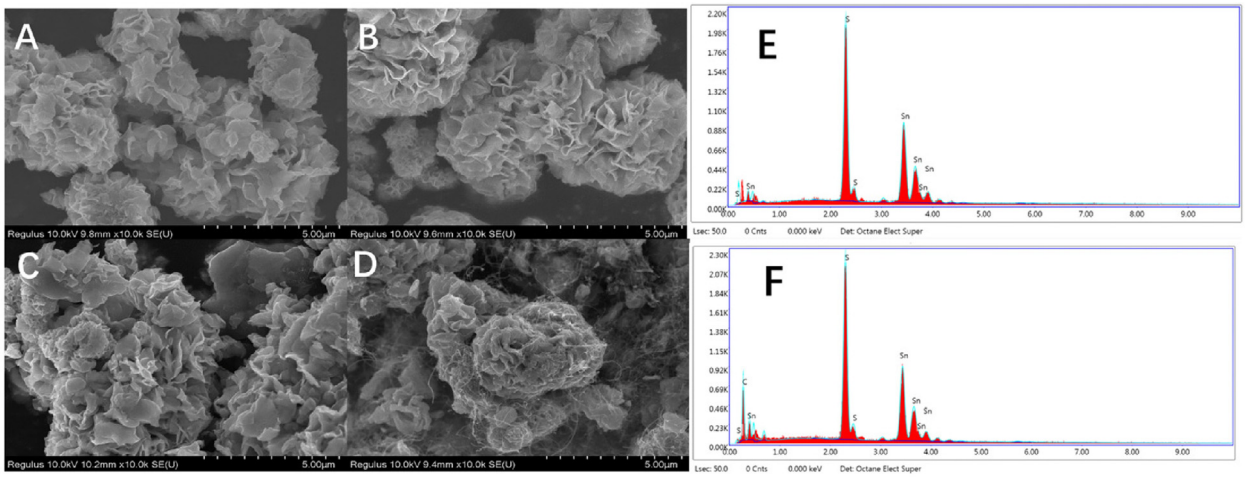

Fig. 3 SEM images of SnS_2 and SnS_2/CNTs: (A) 4h-SnS_2, (B) 6h-SnS_2, (C) 8 h-SnS_2, (D) 4h-SnS_2/CNTs, and SEM-EDS spectra of (E) 4h-SnS_2 and (F) 4h-SnS_2/CNTs.

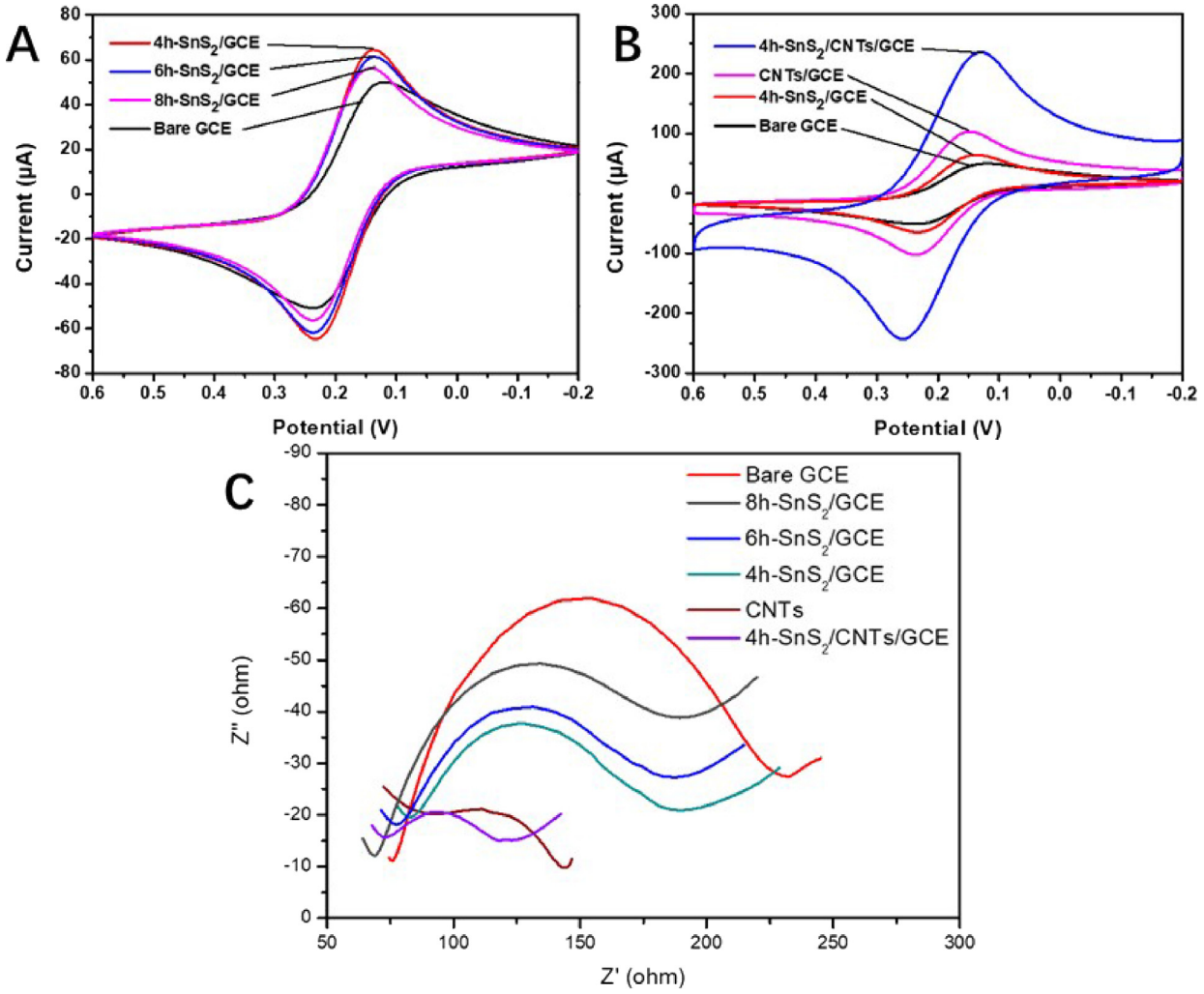

Fig. 4 CV and EIS of different electrodes in 0.1 mol/L of KCl solution containing 5 mmol/L of $K[Fe(CN)_6]^{3-/4-}$ at a scan rate of 100 mV/s: (A) GCE, 4h-SnS_2/GCE, 6h-SnS_2/GCE, 8h-SnS_2/GCE, (B) GCE, 4h-SnS_2/GCE, CNTs/GCE, 4h-SnS_2/CNTs/GCE and (C) EIS of different modified electrodes recorded.

peak currents and peak potentials. As discernible in Fig. 4A, the redox peak current of Fe^{2+}/Fe^{3+} pairs for bare GCE was the smallest, whereas the redox peak current of SnS_2/GCE was slightly higher, indicating that tin disulfide had a catalytic effect on the redox reaction. Moreover, the peak current of 4h-SnS_2/GCE was found to be the largest, followed by 6h-SnS_2/GCE and 8 h-SnS_2/GCE. These results support that smaller particle sizes correspond to larger specific surface areas, and thus better electron transfer ability and stronger conductivity. Bare GCE was modified with CNTs to further enhance its current response and results were as illustrated in Fig. 4B. As it was apparent that the electrochemical performance of CNTs was better than that of SnS_2, 4h-SnS_2 nanoparticles were combined with CNTs to form a 4h-SnS_2/CNTs composite. The modified electrode based on 4h-SnS_2/CNTs (4h-SnS_2/CNTs/GCE) had the highest response because 4h-SnS_2/CNTs had excellent electrocatalytic ability for Fe^{2+}/Fe^{3+} pairs.

Electrochemical impedance spectroscopy (EIS) can provide useful information regarding impedance changes on the electrode surface during the fabrication process, further verifying its results (Fig. 4C). The charge-transfer resistance was related to the electron-transfer kinetics of the redox probe ($[Fe(CN)_6]^{3-}/[Fe(CN)_6]^{4-}$) at the electrode interface and could be estimated from the diameter of the semicircular part of the EIS curve. Fig. 4C illustrates the typical Nyquist plots obtained from bare GCE, 8h-SnS_2/GCE, 6h-SnS_2/GCE, 4h-SnS_2/GCE, CNTs/GCE, and 4h-SnS_2/CNTs/GCE in aqueous KCl (0.1 mol/L) containing 5.0 mmol/L $[Fe(CN)_6]^{3-}/[Fe(CN)_6]^{4-}$. A large diameter of the semicircle part was observed for GCE. The diameter of the semicircle was reduced when the GCE surface was coated with SnS_2 nanoparticles due to improved electrical conductivity. In addition, the smaller surface area facilitated electron transport, and thus the semicircle diameter of 4h-SnS_2/GCE was much smaller. The semicircle diameter showed an even greater decrease in CNTs/GCE due to the excellent electron transfer ability of the carbon nanotubes. The electrochemical impedance spectrum of 4h-SnS_2/CNTs/GCE had the smallest semicircle diameter, which proved that the fastest electron-transfer kinetics of $[Fe(CN)_6]^{3-/4-}$ occurred in 4h-SnS_2/CNTs/GCE rather than in the other modified electrodes. The EIS results were in full agreement with the CV results.

To understand the electrochemical behavior of each modified electrode, the electrochemically active surface area (A) of each electrode could be derived from Randles Sevcik Eq. (1) (Zhang et al., 2020; Rao et al., 2018; Prasad et al., 2017):

$$Ip = 268600n^{3/2}AD^{1/2}CV^{1/2} \quad (1)$$

where Ip is the peak current (A), n is the number of electrons exchanged during the electron transfer process, A is the active surface area (cm^2), D is the diffusion coefficient (cm^2/s), C is the concentration (mol/cm^3), and V is the scan rate (1/Vs). Because the effective physical radius was 1.5 mm, the value of the electrochemically active surface area of 4h-SnS_2/CNTs/GCE could be estimated as 0.30 cm^2, which was 4.23 times that of GCE. The high electrocatalytic properties could be attributed to the large surface area as well as the greater electron transfer capability of 4h-SnS_2/CNTs/GCE compared to the other electrodes.

3.2.2. Electrochemical responses of various modified electrodes in rutin solutions

The CV curves of bare GCE and various modified electrodes in 5 μmol/L of rutin in 0.05 mol/L PBS (pH 3.0) were as shown in Fig. 5. At a scanning rate of 100 mV/s, a reduction peak was observed at 0.48 V and the electrochemical responses of the SnS_2-modified electrodes to rutin were each slightly different (Fig. 5A). The response current of rutin in 4h-SnS_2/GCE with the smallest particle size was found to be the largest, which suggested that it was the most suitable material for electrodes. As evident in Fig. 5B, the response currents of GCE, 4h-SnS_2/GCE, CNTs/GCE, and 4h-SnS_2/CNTs/GCE increased significantly. The 4h-SnS_2/CNTs composite had a large specific surface area and good conductivity. Hence, faster electron transfer in the electrode was due to improved catalytic efficiency.

3.3. Optimization of electrochemical experimental conditions

3.3.1. Effect of buffer solution pH

The pH value of the buffer solution is considered a significant influential factor that will influence on the results of electro-

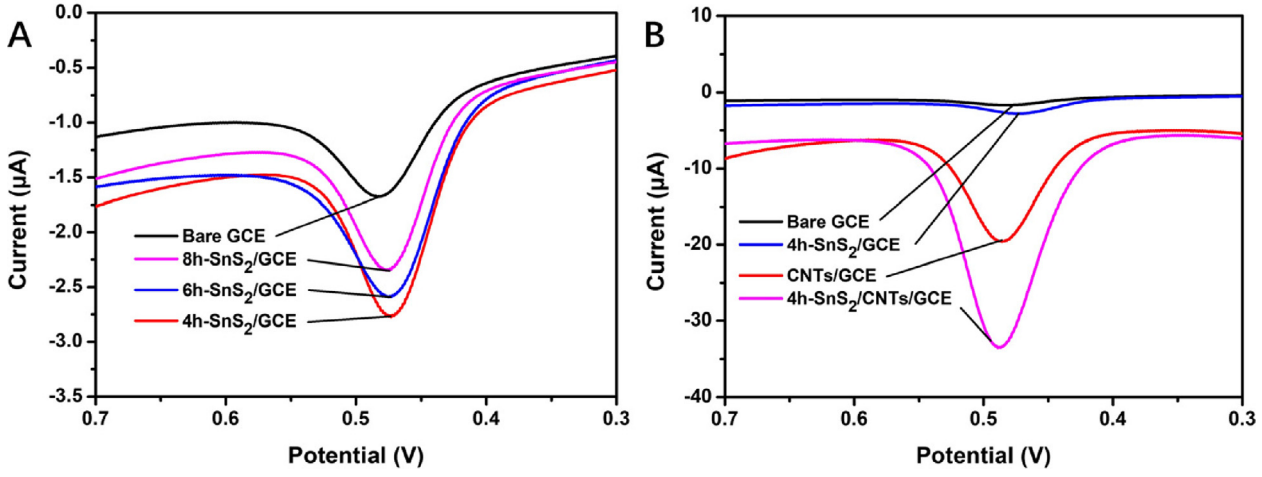

Fig. 5 CV of different electrodes in 5 μmol/L of rutin in 0.05 mol/L PBS (pH 3.0) at a scan rate of 100 mV/s: (A) SnS_2-modified electrodes and (B) modified electrodes.

chemical detection. Therefore, it was necessary to select the appropriate pH of PBS to optimize the sensitivity for rutin determination. As shown in Fig. 6, increase in the pH of the buffer solution moved the peak potential of rutin moved in the negative direction. A linear relationship was observed between the values of potential and pH and could be expressed as $potential = -0.0530\ pH + 0.6219$ ($R^2 = 0.9947$). The slope in this relationship (53 mV/pH) approximated the theoretical value of -59 mV/pH. This indicated that the proton number and electron transfer number involved in rutin oxidation on 4h-SnS_2/CNTs/GCE electrodes were equal, implying that it possibly followed the 2-electron-2-proton mechanism (El Jaouhari et al. 2020). According to Scheme 1, the electrochemical oxidation mechanism of rutin involved several rapid and continuous stages, which was first triggered by electron transfer to produce phenoxy radicals in the form of four mesomeric intermediates (A-D). Due to the electronic effects of the hydroxyl groups, the structure of radical B was the most stable. However, it instantly experienced electron transfer once more, producing the carbocation, and then was dehydrated rapidly, transforming into the final product 30, 40-diquinone (E), which could be reduced to the original rutin in the reverse reaction

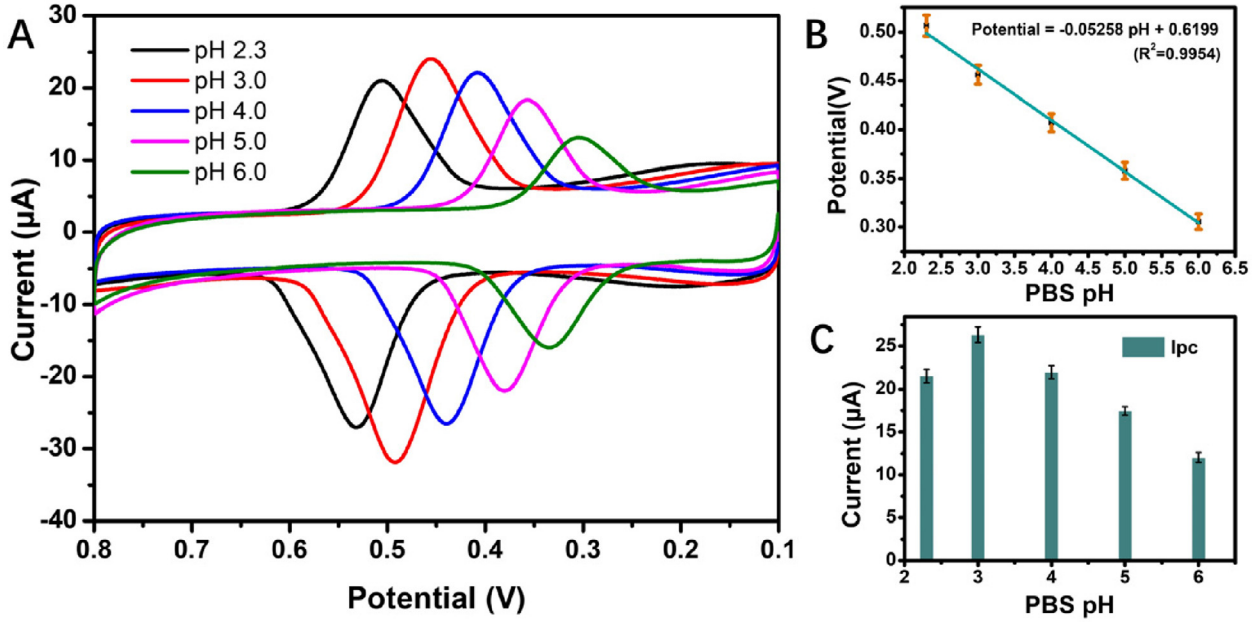

Fig. 6 (A) CV of 5.0 μmol/L of rutin in 0.05 mol/L pH phosphate buffer solutions (pH = 2.3, 3, 4, 5, 6) at a scan rate of 100 mV/s; (B) effects of different pH values on the peak potential, and (C) effects of different pH values on the peak current.

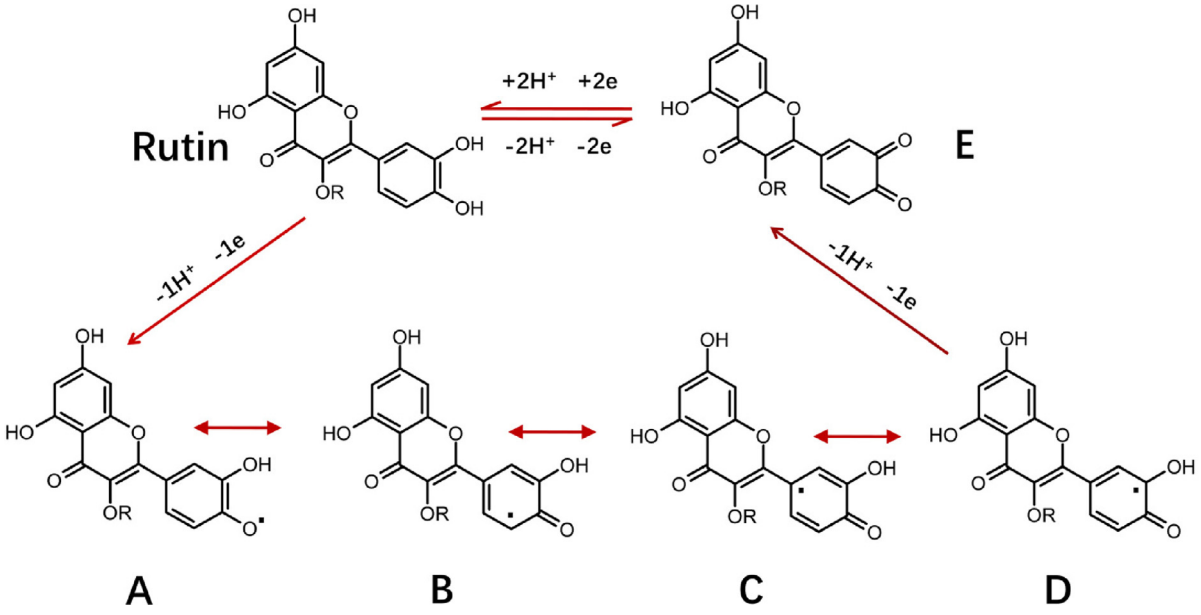

Scheme 1 Electrochemical oxidation mechanism of rutin.

(Zhang et al., 2015; Sun et al., 2008). Moreover, the peak current first increased and then decreased as the pH of the buffer solution increased, which indicated that the electrode reaction of rutin required the participation of protons. Rutin has four phenolic hydroxyl groups, which have difficulty reacting electrochemically due to the lack of protons under alkaline conditions. The optimal pH of buffer solution was selected to be 3 based on the pH at which the largest peak current was achieved.

3.3.2. Effect of 4h-SnS_2/CNTs dosage

The peak current of rutin will also be affected by the extent of modification to a composite. Generally, the larger the specific surface area of the electrode material, the higher the number of active sites in the electrode. However, when a high amount of modified material results in an overly thick modified film, electron transfer in the electrode is hindered and the electrochemical response is reduced. Therefore, it is necessary to control the dosage of 4h-SnS_2/CNTs composite to improve its sensitivity to rutin (Fig. S2). When 5 μL of the modified materials was used, 4h-SnS_2/CNTs/GCE had the highest response to rutin. However, its electrochemical response decreased as the thickness of the modified layer increased due to the restriction to the ionic transfer rate with excessive materials. Therefore, 5.0 μL of 4h-SnS_2/CNTs nanocomposites was considered the optimal amount to promote electrochemical activity with extensive active sites and edges.

3.3.3. Effects of scanning rate and the mechanism of electro surface reaction

An increase in scanning rate from 40 mV/s to 180 mV/s resulted in not only the substantial enhancement of the oxidation and reduction peak current of rutin (Fig. 7), but also a linear movement towards the negative potential in the oxidation and reduction peak current, demonstrating that the surface of 4h-SnS_2/CNTs/GCE had improved adsorption capacity and electron transfer kinetics. The linear relationship between the anodic peak current (*Ipa*) and cathodic peak current (*Ipc*) could be expressed as *Ipa* (μA) = -0.2567*v* (mV/s) - 1.6664 (R^2 = 0.9992) and *Ipc* (μA) = 0.2181*v* (mV/s) + 0.3506 (R^2 = 0.9998). These results indicated that the electrochemical behavior of rutin on 4h-SnS_2/CNTs/GCE exhibited adsorption-controlled electron transfer without any fouling effect (El Jaouhari et al. 2020; Yao et al., 2019; Chen et al. 2019). As the scanning rate decreased, the current response of rutin decreased and the sensitivity worsened. In contrast, as the scanning rate increased, the current response and sensitivity both increased, whereas reversibility of the redox reaction decreased. Therefore, the optimal scanning rate was determined to be 100 mV/s.

3.4. Linearity, interference, reproducibility, and stability

To explore the electrochemical performance of 4h-SnS_2/CNTs/GCE, DPV was applied to determine the concentration of rutin in optimal experimental conditions, with results as shown in Fig. 8. The optimal concentrations of rutin were 0.005-0.05 μmol/L and 0.1-6.0 μmol/L. A linear relationship was observed between the *Ipa* and concentration (*C*) of 4h-SnS_2/CNTs/GCE. At low concentrations, this relationship could be expressed as the equation *Ipa* (μA) = -37.85*C* (μmol/L) - 0.0162 (R^2 = 0.9947), and at high concentrations, as *Ipa* (μA) = -20.24*C* (μmol/L) - 0.9073 (R^2 = 0.9857). According to the signal measured in the blank solution, which was determined using the SnS_2/CNTs electrochemical sensor measuring 6 times in parallel, the current was about 0.019 μA (Fig. S3). Based on the equation *Ipa* (μA) = -37.85*C* (μmol/L) - 0.0162 (R^2 = 0.9947) as well as the relationship between the current signal of lowest detection limit and the noise signal (S/N = 3), the limit of detection (LOD) was calculated to be 0.22 nmol/L.

It was also found that compared to other common methods of rutin detection, the electrochemical method used in this experiment had the lowest detection limit and the highest sensitivity (Table 1). Therefore, the proposed electrochemical method was fast, simple, and sensitive for rutin determination.

In real sample analysis, the interference of unknown substances is inevitable, thus, anti-interference is an important characteristic of modified electrodes. Ions and molecules that might interfere with the experiment were added to measure the electrochemical response of 4h-SnS_2/CNTs/GCE. The interference of the 4h-SnS_2/CNTs modified electrode was

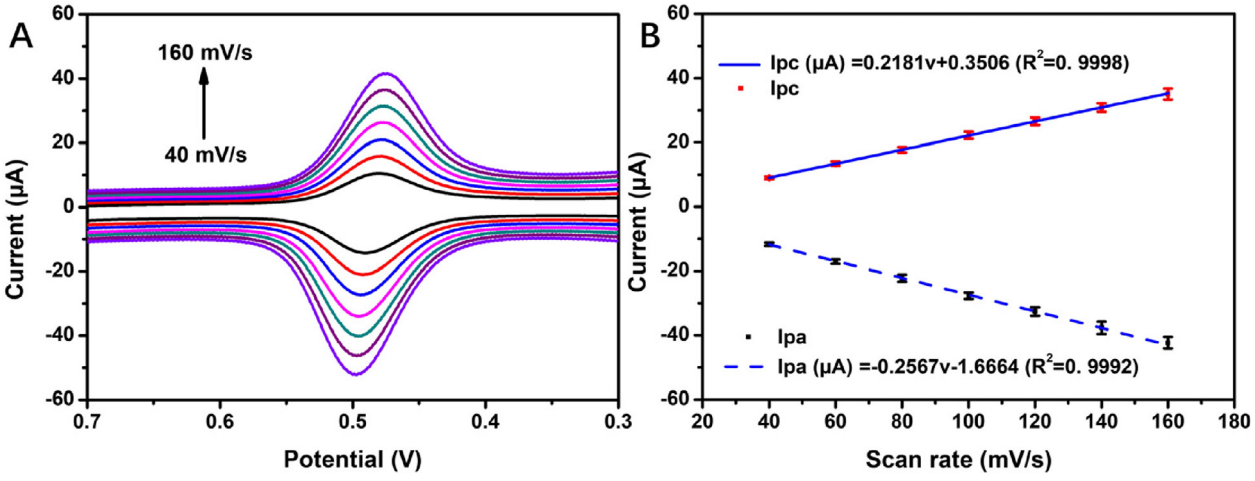

Fig. 7 (A) CV of 5.0 μmol/L of rutin in 0.05 mol/L PBS (pH 3.0) at different scanning rates (40 mV/s, 60 mV/s, 80 mV/s, 100 mV/s, 120 mV/s, 140 mV/s, and 160 mV/s); (B) linear relationship between the scanning rate and response peak current.

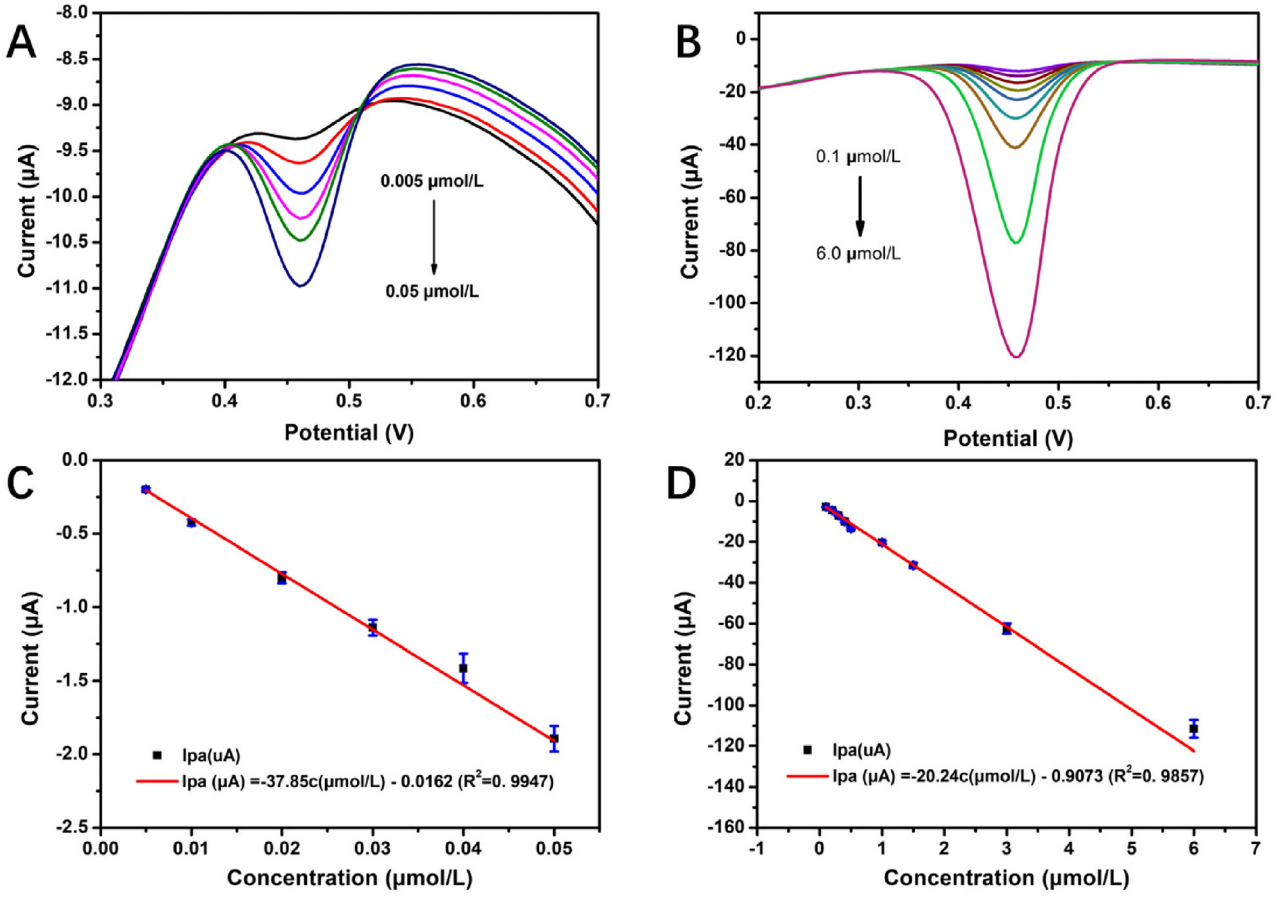

Fig. 8 DPV curves in 0.05 mol/L PBS (pH 3.0) at a scan rate of 100 mV/s for rutin concentrations of (A) 0.005–0.050 μmol/L and (B) 0.1–6.0 μmol/L, (C) standard curve in the low concentration range of rutin (0.005–0.050 μmol/L), and (D) standard curve in the high concentration range of rutin (0.1–6.0 μmol/L).

Table 1 Performances of different methods for rutin detection.

Detection method	Innovation	LOD (mol/L)	Reference
Capillary electrophoresis	Response surface methodology	4.97×10^{-6}	Martí et al., 2017
	Photodiode array detector.	5.45×10^{-7}	Memon et al., 2017
Fluorescence spectrometry	Cysteine-stabilized copper nanoclusters	21×10^{-8}	Wang et al., 2016
	MoS_2 quantum dots	3.50×10^{-7}	Sun et al., 2020
High-performance liquid chromatography	UHPLC/ESI-Q-TOF-MS/MS	1.35×10^{-7}	Ahmad et al., 2016
	Modified QuEChERS method	1.20×10^{-7}	Rotta et al., 2019
Electrochemical method	Cu_2O-Au/nitrogen-doped graphene nanocomposites	3×10^{-8}	Li et al., 2017
	rGO-InTAPc/GCE	2×10^{-9}	Shi et al., 2022
	SnS_2/CNTs/GCE sensor	1.67×10^{-9}	This report

explored in solutions of 5 μmol/L rutin, with the presence of ions (50-fold concentration) or organic substances (10-fold concentration). As shown in Fig. 9, I0 and I were the Ipa of rutin in 5 μmol/L solutions before and after adding the interferents, respectively. The results suggested that the interferents had no significant impact on the determination of rutin by 4h-SnS_2/CNTs/GCE, which indicated good selectivity for rutin in the electrodes.

The storage stability test was investigated by DPV in a solution of 5.0 μM rutin. Notably, after 10 days of storage, the peak current was reduced by 8.2 %. Furthermore, the repeatability was assessed using the same 4h-SnS_2/CNTs/GCE after 6 successive tests (RSD $\leq$ 3.83 %), and reproducibility was calculated 6 times using 6 different 4h-SnS_2/CNTs/GC (RSD $\leq$ 4.18 %). The above results verified that the sensor has reliable electrochemical performance.

3.5. Analysis of real samples

After the synthesis and optimization of 4h-SnS_2/CNTs, a 4h-SnS_2/CNTs/GCE sensor was fabricated to detect rutin in medicine samples. This sensor was applied to detect trace levels of

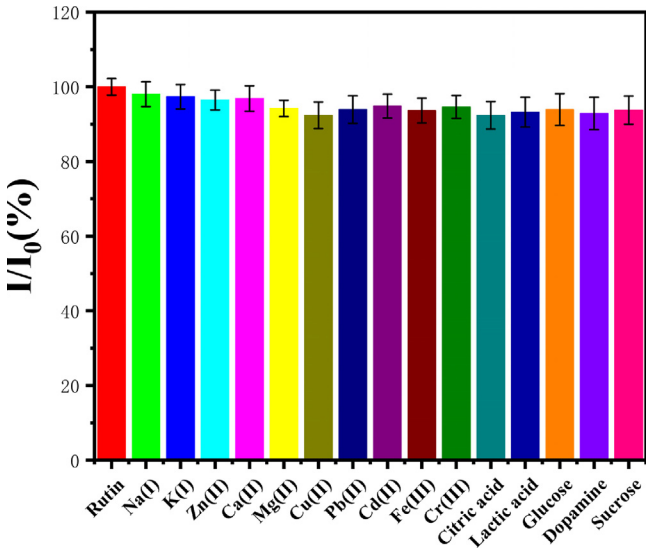

Fig. 9 Selectivity of 4h-SnS_2/CNTs/GCE toward rutin.

rutin in real samples. Twenty tablets of rutin were weighed to be 1.8481 g in total, and the average weight of each was 92.41 mg. The content of rutin in 1 g tablets was 0.2164 g, and 1.099 μmol/L of rutin solution was prepared from a small amount of powder. The peak current response for 4h-SnS_2/CNTs/GCE was calculated, and the average rutin concentration was 1.06 μmol/L (RSD $\leq$ 3.58 %). When the tablets were spiked with three levels of rutin (5.00 μM, 10.00 μM, and 15.00 μM), the recoveries ranged between 96.6 % and 102.3 % (RSD $\leq$ 3.5 %, n = 5) (Table 2). Therefore, the 4h-SnS_2/CNTs/GCE delivered good analytical performance in terms of sensitivity, precision, and accuracy for rutin detection in medicine samples.

Additionally, the practicability of the 4h-SnS_2/CNTs/GCE sensor was explored by analysis of nine different natural plants prepared as described in section 2.6. The DPV and HPLC results under optimal conditions were as presented in Table 3. Noticeably, results from DPV and HPLC analyses were in strong agreement. This validated that the 4h-SnS_2/CNTs/GCE sensor had excellent analytical performance in terms of precision and could be applied the quantification of rutin in plant samples.

Table 3 Results of rutin determination in real plant samples.

Samples	Average concentration (μM)	
	DPV	HPLC
Red date	98.71 ± 4.73	101.23
Black fruit wolfberry	272.82 ± 18.63	280.09
Asparagus	676.29 ± 19.15	673.85
Wolfberry	430.63 ± 22.91	422.26
Grape peel	291.96 ± 6.05	293.69
Tangerine	217.50 ± 5.87	215.23
Eggplant peel	268.94 ± 13.38	280.09
Buckwheat	53.13 ± 1.48	55.69
Apple	55.42 ± 3.47	57.98

Table 2 Recovery rates of rutin in tablets.

Samples	Rutin spiked (μM)	Rutin found (μM)	Recovery (%)	RSD (n = 5, %)
Rutin tablets	0.00	1.06	–	3.58
	5.00	6.83	96.6	3.29
	10.00	11.23	102.3	3.41
	15.00	16.18	101.2	3.19

4. Conclusion

In summary, a rapid and selective electrochemical sensor was proposed and synthesized in this study for the determination of rutin concentration. Nanoflower-like structured SnS_2 was successfully synthesized and composited with multi-walled carbon nanotubes via simple sonochemical treatments. The prepared SnS_2/CNTs modified electrode was then verified to possess higher effectiveness in the electrochemical determination of rutin, exhibiting a good linear range from 0.005 - 0.05 μmol/L and 0.1–6.0 μmol/L with an LOD value of 0.22 nmol/L (S/N = 3). In contrast to previous methods, the proposed sensor is characterized by good anti-interference properties, superior reproducibility and repeatability, and long-term stability. Moreover, the fabricated sensor was successfully applied to determine rutin not only in commercially available rutin tablets, but also in natural vegetation to evaluate the medicinal value of plants. Therefore, this strategy could be further applied to the development of sensing devices for analyze different substances.

CRediT authorship contribution statement

Ying Liang: Conceptualization, Methodology, Investigation, Formal analysis, Validation, Visualization, Writing – original draft, Funding acquisition. **Lingyu Zhang:** Formal analysis, Investigation, Validation. **Hongmei Wang:** Formal analysis, Investigation, Validation. **Xinru Cai:** Formal analysis, Investigation, Validation. **Li Zhang:** Formal analysis, Investigation, Validation. **Yixin Xu:** Formal analysis, Investigation, Validation. **Chunxia Yao:** Conceptualization, Methodology, Investigation, Formal analysis, Validation, Visualization, Funding acquisition. **Wenshuai Si:** Conceptualization, Resources, Supervision, Methodology, Project administration. **Zhipeng Huang:** Conceptualization, Resources, Supervision, Methodology, Project administration. **Guoyue Shi:** Conceptualization, Resources, Supervision, Methodology, Project administration.

Declaration of Competing Interest

The authors declare that they have no known competing financial interests or personal relationships that could have appeared to influence the work reported in this paper.

Funding

This work was supported by the Foundation of Shanghai Municipal Commission of Science & Technology Commission (20392002200) and the Fundamental Research Funds of Shanghai University of Medicine & Health Sciences (HXXM-20-07-004, SSF-21-07-001).

Appendix A. Supplementary material

Supplementary data to this article can be found online at https://doi.org/10.1016/j.arabjc.2023.104613.

References

Ahmad, N., Ahmad, R., Naqvi, A.A., Alam, M.A., Samim, M., Iqbal, Z., Ahmad, F.J., 2016. Quantification of rutin in rat's brain by UHPLC/ESI-Q-TOF-MS/MS after intranasal administration of rutin loaded chitosan nanoparticles. EXCLI J. 15, 518. https://doi.org/10.17179/excli2016-361.

Al-Harbi, N.O., Imam, F., Al-Harbi, M.M., Al-Shabanah, O.A., Alotaibi, M.R., Sobeai, H.M.A., Afzal, M., Kazmi, I., Al-Rikabi, A.C., 2019. Rutin inhibits carfilzomib-induced oxidative stress and inflammation via the NOS-mediated NF-κB signaling pathway. Inflammopharmacology 27, 817–827. https://doi.org/10.1007/s10787-018-0550-5.

Chen, Y., Huang, W., Chen, K., Zhang, T., Wang, Y., Wang, J., 2019. Facile fabrication of electrochemical sensor based on novel core-shell PPy@ZIF-8 structures: enhanced charge collection for quercetin in human plasma samples. Sens. Actuators B 290, 434–442. https://doi.org/10.1016/j.snb.2019.04.006.

Clancy, A.J., Bayazit, M.K., Hodge, S.A., Skipper, N.T., Howard, C. A., Shaffer, M., 2018. Charged carbon nanomaterials: redox chemistries of fullerenes, carbon nanotubes, and graphenes. Chem. Rev. 118, 7363–7408. https://doi.org/10.1021/acs.chemrev.8b00128.

Diao, M., Li, H., Hou, R., Liang, Y., Wang, J., Luo, Z., Huang, Z., Zhang, C., 2020. Vertical heterostructure of SnS–MoS_2 synthesized by sulfur-preloaded chemical vapor deposition. ACS Appl. Mater. Interfaces 12 (6), 7423–7431. https://doi.org/10.1021/acsami.9b19495.

Huang, F., Meng, R., Sui, Y., Wei, F., Qi, J., Meng, Q., He, Y., 2018. One-step hydrothermal synthesis of a CoS_2@MoS_2 nanocomposite for high-performance supercapacitors. J. Alloy. Compd. 742, 844–851. https://doi.org/10.1016/j.jallcom.2018.01.324.

Incebay, H., Kilic, A., 2022. Electrochemical determination of indigo carmine in food and water samples using a novel platform based on chiral amine-bis (phenolate) boron complex. Dyes Pigm. 197,. https://doi.org/10.1016/j.dyepig.2021.109921 109921.

İncebay, H., Yazıcıgi, l.Z., 2017. Effect of different copper salts on the electrochemical determination of Cu (II) by the application of the graphene oxide-modified glassy carbon electrod. Surf. Interfaces 9, 160–166. https://doi.org/10.1016/j.surfin.2017.09.004.

Jaouhari El, A, Yan, L., Zhu, J., Zhao, D., Khan, M., Liu, X., 2020. Enhanced molecular imprinted electrochemical sensor based on zeolitic imidazolate framework/reduced graphene oxide for highly recognition of rutin. Anal. Chim. Acta 1106, 103–114. https://doi.org/10.1016/j.aca.2020.01.039.

Jiang, Y., Feng, Y., Xi, B., Kai, S., Mi, K., Feng, J., Zhang, J., Xionga, S., 2016. Ultrasmall SnS_2 nanoparticles anchored on well-distributed nitrogen-doped graphene sheets for Li-ion and Na-ion batteries. J. Mater. Chem. A 4 (27), 10719–10726. https://doi.org/10.1039/C6TA03580A.

Jjgyasa, J.K., 2018. Bio-polyphenols promoted green synthesis of silver nanoparticles for facile and ultra-sensitive colorimetric detection of melamine in milk. Biosens. Bioelectron. 120 (30), 153–159. https://doi.org/10.1016/j.bios.2018.08.054.

Kalinová, J.P., Vrchotová, N., Tříska, J., 2018. Contribution to the study of rutin stability in the achenes of Tartary buckwheat (Fagopyrum tataricum). Food Chem. 258, 314–320. https://doi.org/10.1016/j.foodchem.2018.03.090.

Kilic, A., Beyazsakal, L., Findik, B.T., Incebay, H., 2020. Synthesis and electrochemical investigation of chiral amine bis (phenolate)-boron complexes: in vitro antibacterial activity screening of boron compounds. Inorg. Chim. Acta 510,. https://doi.org/10.1016/j.ica.2020.119777 119777.

Kubendhiran, S., Sakthivel, R., Chen, S.M., Mutharani, B., Chen, T.-W., 2018a. Innovative strategy based on a novel carbon-black− β-cyclodextrin nanocomposite for the simultaneous determination of the anticancer drug flutamide and the environmental pollutant 4-nitrophenol. Anal. Chem. 90 (10), 6283–6291. https://doi.org/10.1021/acs.analchem.8b00989.

Kubendhiran, S., Thirumalraj, B., Chen, S.M., Karuppiah, C., 2018b. Electrochemical co-preparation of cobalt sulfide/reduced graphene oxide composite for electrocatalytic activity and determination of H_2O_2 in biological samples. J. Colloid Interface Sci. 509, 153–162. https://doi.org/10.1016/j.jcis.2017.08.087.

Li, S., Yang, B., Wang, C., Wang, J., Feng, Y., Yan, B., Xiong, Z., Du, Y., 2017. A facile and green fabrication of Cu_2O-Au/NG nanocomposites for sensitive electrochemical determination of rutin. J. Electroanal. Chem. 786, 20–27. https://doi.org/10.1016/j.jelechem.2017.01.001.

Liang, Y., Li, H., Hou, R., Wang, J., Wang, K., Ge, M., Luo, J., Huang, Z., Zhang, C., 2019. Vertical stacking of copper sulfide nanoparticles and molybdenum sulfide nanosheets for enhanced nonlinear absorption. ACS Appl. Mater. Interfaces 11 (39), 35835–35844. https://doi.org/10.1021/acsami.9b06662.

Liang, Y., Wang, H., Xu, Y., Pan, H., Guo, K., Zhang, Y., Chen, Y., Liu, D., Zhang, Y., Yao, C., Yu, Y., Shi, G., 2022. A novel molecularly imprinted polymer composite based on polyaniline nanoparticles as sensitive sensors for parathion detection in the field. Food Control 133,. https://doi.org/10.1016/j.foodcont.2021.108638 108638.

Liao, J., Qu, B., Liu, D., Zheng, N., 2015. New method to enhance the extraction yield of rutin from Sophora japonica using a novel ultrasonic extraction system by determining optimum ultrasonic frequency. Ultrason. Sonochem. 27, 110–116. https://doi.org/10.1016/j.ultsonch.2015.05.005.

Liu, Y., Qiu, G., Kong, D., Hu, B., Li, Y., Su, J., Xia, C., 2017b. Strain effect on SnS_2 nanoribbons: robust direct bandgap of zigzag-edge and sensitive indirect semiconductor with armchair-edge states. Superlattice. Microst. 111, 480–486. https://doi.org/10.1016/j.spmi.2017.07.005.

Liu, Z., Xue, Q., Guo, Y., 2017a. Sensitive electrochemical detection of rutin and isoquercitrin based on SH-β-cyclodextrin functionalized graphene-palladium nanoparticles. Biosens. Bioelectron. 89 (12), 444–452. https://doi.org/10.1016/j.bios.2016.04.056.

Martí, R., Valcárcel, M., Herrero-Martínez, J.M., Cebolla-Cornejo, J., Roselló, S., 2017. Simultaneous determination of main phenolic acids and flavonoids in tomato by micellar electrokinetic capillary electrophoresis. Food Chem. 221, 439–446. https://doi.org/10.1016/j.foodchem.2016.10.105.

Memon, A.F., Solangi, A.R., Memon, S.Q., Mallah, A., Memon, N., Memon, A.A., 2017. Simultaneous determination of quercetin, rutin, naringin, and naringenin in different fruits by capillary zone electrophoresis. Food Anal. Methods 10 (1), 83–91. https://doi.org/10.1007/s12161-016-0552-0.

Mondal, S., Sahoo, L., Vinod, C.P., Gautam, U.K., 2021. Facile transfer of excited electrons in Au/SnS_2 nanosheets for efficient solar-driven selective organic transformations. Appl Catal B 286,. https://doi.org/10.1016/j.apcatb.2021.119927 119927.

Pham, V.D., Repain, V., Chacon, C., Bellec, A., Girard, Y., Rousset, S., Campidelli, S., Lauret, J.-S., Voisin, C., Terrones, M., Santos, M.C., Lagoute, J., 2017. Properties of functionalized carbon nanotubes and their interaction with a metallic substrate investigated by scanning tunneling microscopy. J. Phys. Chem. C 121 (43), 24264–24271. https://doi.org/10.1021/acs.jpcc.7b06890.

Prasad, B.B., Kumar, A., Singh, R., 2017. Synthesis of novel monomeric graphene quantum dots and corresponding nanocomposite with molecularly imprinted polymer for electrochemical detection of an anticancerous ifosfamide drug. Biosens. Bioelectron. 94, 1–9. https://doi.org/10.1016/j.bios.2017.02.028.

Rao, H., Liu, X., Ding, F., Wan, Y., Zhao, X., Liang, R., Zou, P., Wang, Y., Wang, X., Zhao, Q., 2018. Nitrogen-doped carbon nanosheet frameworks decorated with Fe and molecularly imprinted polymer for simultaneous detection of mebendazole and catechol. Chem. Eng. J. 338, 478–487. https://doi.org/10.1016/j.cej.2018.01.064.

Reznik, D., Olk, C.H., Neumann, D.A., Copley, J.R.D., 1995. X-ray powder diffraction from carbon nanotubes and nanoparticles. Phys. Rev. B 52 (1), 116. https://doi.org/10.1103/PhysRevB.52.116.

Rotta, E.M., Rodrigues, C.A., Jardim, I.C.S.F., Maldaner, L., Visentainer, J.V., 2019. Determination of phenolic compounds and antioxidant activity in passion fruit pulp (Passiflora spp.) using a modified QuEChERS method and UHPLC-MS/MS. LWT 100, 397–403. https://doi.org/10.1016/j.lwt.2018.10.052.

Sakthivel, R., Kubendhiran, S., Chen, S.-M., Kumar, J.V., 2019. Rational design and facile synthesis of binary metal sulfides VS_2-SnS_2 hybrid with functionalized multiwalled carbon nanotube for the selective detection of neurotransmitter dopamine. Anal. Chim. Acta 1071, 98–108. https://doi.org/10.1016/j.aca.2019.04.058.

Sasikumar, T., Ilanchelian, M., 2021. Water-soluble luminescent copper nanoclusters as a fluorescent quenching probe for the detection of rutin and quercetin based on the inner filter effect. Luminescence 36 (2), 326–335. https://doi.org/10.1002/bio.3945.

Saylakcı, R., Incebay, H., 2021. An electrochemical platform of tannic acid and carbon nanotubes for the sensitive determination of the antipsychotic medication clozapine in pharmaceutical and biological samples. J. Electroanal. Chem. 898,. https://doi.org/10.1016/j.jelechem.2021.115638 115638.

Sghaier, M.B., Pagano, A., Mousslim, M., Ammari, Y., Kovacic, H., Luis, J., 2016. Rutin inhibits proliferation, attenuates superoxide production and decreases adhesion and migration of human cancerous cells. Biomed. Pharmacother. 84, 1972–1978. https://doi.org/10.1016/j.biopha.2016.11.001.

Shi, Y., Chao, L., Mei, L., Chen, Z., Li, X., Miao, M., 2022. Soluble tetraaminophthalocyanines indium functionalized graphene platforms for rapid and ultra-sensitive determination of rutin in Tartary buckwheat tea. Food Control 132,. https://doi.org/10.1016/j.foodcont.2021.108550 108550.

Sun, Y., He, W., Sun, X., Liu, B., 2020. MoS_2 quantum dots as a specific fluorescence sensor for selection of rutin and for temperature sensing. Luminescence 35 (8), 1416–1423. https://doi.org/10.1002/bio.3906.

Sun, W., Yang, M., Li, Y., Jiang, Q., Liu, S., Jiao, K., 2008. Electrochemical behavior and determination of rutin on a pyridinium-based ionic liquid modified carbon paste electrode. J. Pharm. Biomed. Anal. 48 (5), 1326–1331. https://doi.org/10.1016/j.jpba.2008.09.014.

Wang, Z., Chen, T., Chen, W., Chang, K., Ma, L., Huang, G., Chen, D., Lee, J.Y., 2013. CTAB-assisted synthesis of single-layer MoS_2-graphene composites as anode materials of Li-ion batteries. J. Mater. Chem. A 1 (6), 2202–2210. https://doi.org/10.1039/C2TA00598K.

Wang, J., Duan, H.-L., Fan, L., Lin, Y.-M., Sun, J.-N., Zhang, Z.-Q., 2021. Magnetic tetraethylenepentamine modified multi-walled carbon nanotubes as matrix clean-up materials for organophosphorus pesticide residues analysis in cucumber. Food Control 124,. https://doi.org/10.1016/j.foodcont.2021.107904 107904.

Wang, W., Lin, P., Ma, L., Xu, K., Lin, X., 2016. Separation and determination of flavonoids in three traditional chinese medicines by capillary electrophoresis with amperometric detection. J. Sep. Sci. 39 (7), 1357–1362. https://doi.org/10.1002/jssc.201501287.

Wang, S., Yang, B., Liu, Y., 2017. Synthesis of a hierarchical SnS_2 nanostructure for efficient adsorption of Rhodamine B dye. J. Colloid Interface Sci. 507, 225–233. https://doi.org/10.1016/j.jcis.2017.07.053.

Xie, M., Zhao, F., Zhang, Y., Xiong, Y., Han, S., 2022. Recent advances in aptamer-based optical and electrochemical biosensors for detection of pesticides and veterinary drugs. Food Control 131,. https://doi.org/10.1016/j.foodcont.2021.108399 108399.

Xu, X., Liu, W., Kim, Y., Cho, J., 2014. Nanostructured transition metal sulfides for lithium ion batteries: Progress and challenges. Nano Today 9 (5), 604–630. https://doi.org/10.1016/j.nantod.2014.09.005.

Xu, L., Zhang, P., Jiang, H., Wang, X., Chen, F., Hu, Z., Gong, Y., Shang, L., Zhang, J., Jiang, K., Chu, J., 2019. Large-scale growth and field-effect transistors electrical engineering of atomic-layer SnS_2. Small 15 (46), 1904116. https://doi.org/10.1002/smll.201904116.

Xue, S.M., Xu, Z.L., Tang, Y.J., Ji, C.H., 2016. Polypiperazine-amide nanofiltration membrane modified by different functionalized multiwalled carbon nanotubes (MWCNTS). ACS Appl. Mater. Interfaces 8 (29), 19135–19144. https://doi.org/10.1021/acsami.6b05545.

Yao, J., Chen, M., Li, N., Liu, C., Yang, M., 2019. Experimental and theoretical studies of a novel electrochemical sensor based on molecularly imprinted polymer and B, N, F-CQDs/AgNPs for enhanced specific identification and dual signal amplification in highly selective and ultra-trace bisphenol S determination in plastic products. Anal. Chim. Acta 1066, 36–48. https://doi.org/10.1016/j.aca.2019.03.051.

Yin, L., Cheng, R., Song, Q., Yang, J., Kong, X., Huang, J., Lin, Y., Ouyang, H., 2019. Construction of nanoflower SnS2 anchored on g-C3N4 nanosheets composite as highly efficient anode for lithium ion batteries. Electrochim. Acta 293, 408–418. https://doi.org/10.1016/j.electacta.2018.10.020.

Zhang, B., Jaouhari, A.E., Wu, X., Liu, W., Zhu, J., Liu, X., 2020. Synthesis and characterization of PEDOT-MC decorated AgNPs for voltammetric detection of rutin in real samples. J. Electroanal. Chem. 877,. https://doi.org/10.1016/j.jelechem.2020.114632 114632.

Zhang, K., Xu, J., Zhu, X., Lu, L., Duan, X., Hu, D., Dong, L., Sun, H., Gao, Y., Wu, Y., 2015. Poly (3, 4-ethylenedioxythiophene) nanorods grown on graphene oxide sheets as electrochemical sensing platform for rutin. J. Electroanal. Chem. 739, 66–72. https://doi.org/10.1016/j.jelechem.2014.12.013.

Zhou, Q., Huang, J., Wang, J., Yang, Z., Liu, S., Wang, Z., Yang, S., 2015. Preparation of a reduced graphene oxide/zirconia nanocomposite and its application as a novel lubricant oil additive. RSC Adv. 5 (111), 91802–91812. https://doi.org/10.1039/C5RA17440F.